

Flame retardant poly(lactic acid) biocomposites reinforced by recycled wool fibers – Thermal and mechanical properties

B. Tawiah¹, B. Yu¹, S. Ullah³, R. Wei², R. K. K. Yuen², J. H. Xin¹, B. Fei^{1*}

¹Institute of Textiles and Clothing (ITC), The Hong Kong Polytechnic University, Hong Kong, China

²Department of Civil and Architectural Engineering, City University of Hong Kong, Kowloon, Hong Kong, China

³Department of Mechanical Engineering, The Hong Kong Polytechnic University, Hong Kong, China

Received 15 January 2019; accepted in revised form 10 March 2019

Abstract. The inherently poor flame retardancy and comparatively low tensile strength of poly(lactic acid) (PLA) have limited its wide adoption as alternative ‘green’ engineering plastic in many fields. This manuscript reports the synthesis of a new phosphorus flame retardant – phenylphosphonic 3(2-aminobenzothiazole) (P-TAB) and its combination with recycled short wool fibers (WF) for improving the flame retardancy and the mechanical properties of PLA. Fourier transform infrared (FTIR), ¹H, and ¹³C nuclear magnetic resonance (NMR) spectra proved that P-TAB was effectively synthesized. Considerable reductions in heat release rate, total heat released, CO and CO₂ produced were attained with 3 wt% P-TAB and various WF loadings. The fire performance index (FPI), and fire growth index (FGI) improved by 38.2 and 48.1% respectively. The composite achieved a V-0 rating at 20 wt% WF loading and an LOI value of 28.5%. TG-IR results showed substantial reductions in evolved gaseous products. The tensile strength and Young’s modulus improved significantly with the increasing content of WF in the composite.

Keywords: polymer composites, flame retardant, cone calorimeter, fiber reinforcement, pyrolysis products

1. Introduction

Polymer composites (PCs) are designed to achieve properties beyond those attainable by homopolymers [1–4]. Among the different classes of PCs, fiber reinforced polymer composites (FRPCs) with thermoplastic polymers are particularly useful in the production of different engineering products due to their light weight and high mechanical properties [5–8]. The most preferred reinforcement material for PCs are often natural fibers because of their biodegradability, low cost, and excellent mechanical properties [9–11]. PCs find applications in different fields including automotive and the aviation industry, buildings and construction, and windmills as blades [9, 12–15]. Considering the high-end engineering applications

of PCs, the need for bio-based FRPCs with improved flame resistance and excellent mechanical properties cannot be overemphasized [9, 16, 17]. PLA is a vital bioplastic with excellent properties, but the issue of high flammability and low thermo-mechanical properties has made it inferior compared to the petrochemically derived plastics [18, 19]. This has limited its applications where high tensile strength and flame resistance is required [20, 21]. Therefore, a mechanically robust FR PLA composite is proposed using phosphorus-nitrogen-sulfur containing FR reinforced by recycled short wool fibers. In this way, a bio-based PLA PC with superior FR performance and exceptional tensile strength can be obtained with properties that can match or exceed the performance

*Corresponding author, e-mail: bin.fei@polyu.edu.hk
© BME-PT

of the traditionally known petrochemically derived PCs.

Wool, a protein-based animal fiber with rich nitrogen and sulfur content [22, 23] possess inherent flame resistance capabilities and does not drip when burning [24, 25]. Also, wool has unique properties such as high ignition temperature, low heat of combustion and a high LOI (ca. 25.2%) [26]. Its flame resistance performance is linked to the dehydration predisposition of the sulfur-containing amino acids and the release of inert nitrogen oxides during combustion leading to the formation of intumescent chars [26–28]. The amino acids and abundant sulfur in WF catalyzes dehydration and the production of char which can limit the possibility of melt dripping commonly associated with PLA. Beyond the inherent FR properties of wool fiber (WF), it also possesses high tensile strength due to its microfibrillated network structure; hence its combination with thermoplastics in recent years for simultaneous mechanical strength and flame resistance enhancement for PCs in recent years [22, 24, 29, 30]. In this manuscript, the conversion of recycled WF for reinforcement of bioplastic PC is proposed together with a new FR – phenylphosphonic tri(2-aminobenzothiazole) (P-TAB) to reduce the incidence of WF waste in the environment.

Phosphorus (P) containing FRs are particularly important due to their high efficiency, low loading, and less corrosive effect on equipment during processing and combustion [31, 32]. As a result, different P containing FRs have been synthesized and applied to different polymers over the years [33, 34]. Recently, P containing FRs with a significant amount of nitrogen (N) and sulfur (S) are deemed to further enhance the condensed phase FR chemistry of polymeric materials during combustion [35, 36]. The P-N-S containing FRs possess unique properties because they function actively in both the condensed and the gas phases to change the typical decomposition route of polymers [36]. Typically, the S moiety degenerates into sulfonic acids during the pyrolysis process to augment and promote char formation of P moiety in the condensed phase. The N component releases inert nitrogen oxides that reduces the burning rate of the polymer in the gas and the condensed phase. Despite the inherent FR performance and high tensile strength of WF, its application as fiber reinforced PLA composites (FRPC) with a new P-N-S containing FR has rarely been reported. P-N-S containing substances are generally eco-friendly because they are the main

constituents of most manure and plants nutrients, and therefore may not cause environmental pollution in landfill sites, considering the fact that PLA is also 100% compostable [37, 38].

This manuscript reports the design and synthesis of a new FR containing a significant amount of P-N-S and its combination with recycled short WF for simultaneous FR and tensile strength enhancement of PLA biocomposites. The FR was synthesized using the $A_3 + B_1$ mechanism and compounded with PLA and WF by means of solvent mixing and compression molding approaches to produce FRPCs. The thermal, crystallization and mechanical FR properties of the FRPCs were investigated extensively, and the FR mechanism was elucidated.

2. Experimental

PLA granules (Bioplus 6201D) was supplied by NatureWorks, 15305 Minnetonka Blvd., Minnetonka, USA. Phosphoryl chloride (POCl_3) (99.5%), pyridine- d_5 , and non-ionic detergent octylphenoxypolyethoxyethanol (NP-40) were supplied by Sigma Aldrich (Germany). 2-Aminobenzothiazole (ABT) (97%), sodium sulfate anhydrous, trimethylamine (TEA), sodium carbonate, and anhydrous tetrahydrofuran (THF) were purchased from Acros Organics (USA). Waste wool fiber (WF) was supplied as a gift by Hengyuanxiang (Group) Co., Ltd, Shanghai, China. The WF was pretreated before mixing with PLA/P-TAB composites.

2.1. Pretreatment of recycled wool fiber

Waste WF was scoured in 1 g/l Na_2CO_3 and 1 g/l NP-40 non-ionic detergent at 60 °C for 30 min to remove dirt. WF was rinsed successively in warm and cold water, squeezed, and dried at room temperature. WF was then cut into an average length of 2–3 mm and homogenized for 10 min. The homogenized WF was further dried in a vacuum oven at 100 °C overnight to attain constant weight before compounding.

2.2. Synthesis of phenylphosphonic 3(2-aminobenzothiazole) (P-TAB)

P-TAB was synthesized according to Figure 1. 2-Aminobenzothiazole (0.3 mol) was dissolved in 40 ml anhydrous THF, discharged into a round bottom flask under stirring in an ice bath during which 0.3 mol TEA was added under low humidity (RH 14). POCl_3 0.1 mol in 10 ml anhydrous THF was added dropwise, and the reaction proceeded in an ice bath for

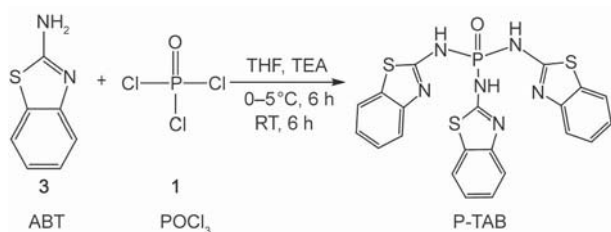


Figure 1. Synthesis of phenylphosphonic 3(2-aminobenzothiazole) (P-TAB).

6 h and then at room temperature for another 6 h. The product was washed severally with THF and DI water to remove the unreacted monomers, and the triethylamine hydrochloride produced until pH 6.5–7 was attained. The pure compound was dried over sodium sulfate anhydrous for 24 h and then in a vacuum oven at 60 °C for 24 h to obtain a product yield of 83.7%. The product (P-TAB) (M_w 494.55) was characterized by ^1H NMR (400 MHz, Pyr) δ 9.25 (d, $J = 8.0$ Hz, 3H), 9.23 (d, $J = 7.9$ Hz, 3H), 9.15 (s, $J = 7.8$ Hz, 3H), 8.82–8.74 (m, 3H), 8.69 (m, 3H), 8.59–8.52 (m, 3H). ^{13}C NMR (101 MHz, Pyr) $\delta = 169.31$, 154.75, 133.30, 127.35, 122.95, 122.59, 120.01.

2.3. Preparation of PLA/P TAB/WF composites

PLA/P-TAB/WF composites were prepared by the combinatory solvent mixing, and the hot compression molding approach similar to the literature [39]. A quantity of P-TAB (see Table 1) was dispersed in 50 ml CHCl_3 and subjected to ultrasonication for 30 min. An amount of PLA (predetermined in Table 1) was also dissolved in 400 ml CHCl_3 with the aid of a mechanical stirrer at 500 r/min. The dispersed P-TAB was mixed with the dissolved PLA under vigorous stirring for 2 h. For samples containing WF, a predetermined quantity of homogenized WF was added in bits (Table 1) and stirred mechanically for 2 h to obtain homogenous PLA/P-TAB/WF composite mixture. The temperature of the PLA/P-TAB/WF composite mixture was increased to 50 °C for some

Table 1. P-TAB and wool fiber (WF) loading.

Sample	PLA [%]	P-TAB [%]	(WF) [%]
Neat PLA	100	–	–
PLA/P-TAB	97	3	–
PLA/P-TAB/WF 3%	92	3	5
PLA/P-TAB/WF 5%	87	3	10
PLA/P-TAB/WF 10%	77	3	20

of the solvent to evaporate. The PLA/P-TAB/WF composite mixture was cast into a mold and dried in an oven at 70 °C for 24 h to remove the remaining solvent. The dried PLA/P-TAB/WF composites were again conditioned at 90 °C for 12 h in a vacuum oven, crushed into pieces and homogenized for 15 minutes. The composite samples without WF were also treated similarly. The composites were pressed with an automatic hydraulic press at 180 °C for 2 min at 10 bars and then degassed. The composite samples were then pressed again for the second time for 1 min at 15 bars at 180 °C and then transferred to the cold part for final pressing for 1 min. The molds are removed to obtain the standard samples. Neat PLA granules were also dissolved and pressed into standard samples using the same procedure. The samples used for the tensile test were prepared and pressed using the same method.

2.4. Characterization

FTIR spectrometer equipped with attenuated total reflection (ATR) accessory was used. The samples were scanned at 4 cm^{-1} after averaging 16 scans between 650–4000 cm^{-1} . ^1H and ^{13}C NMR spectra of P-TAB was recorded with AVANCE 300 Bruker spectrometer (Germany), using Pyridine- d_5 as a solvent. A Mettler Toledo TGA/DSC 1 Star System, was used to study the thermal properties of P-TAB and PLA/P-TAB/WF composites at 20 °C/min with air flow rate of 40 ml/min between 40–700 °C and samples weight 4–5 mg. A Perkin Elmer DSC 800 instrument was used at a scanning rate of 10 °C/min under N_2 atmosphere with samples (4–5 mg) heated from 30 to 200 °C and cooled to 30 °C, after which second heating was applied following the same program. The degree of crystallinity (χ_c) was calculated based on ΔH_m according to Equation (1):

$$\chi_c = \frac{\Delta H_m}{\Delta H_{mp}(1-x)} \cdot 100\% \quad (1)$$

where ΔH_m is the melting enthalpy of neat PLA and PLA/P-TAB/WF composites, ΔH_{mp} is the melting enthalpy of 100% crystalline PLA (93.6 J/g), and x is the FR/WF content [40].

A TESCAN VEGA 3 SEM was used to observe the fracture surface and the char residues at various magnifications after sputter coating with Au. Residual chars of PLA/P-TAB/WF composites were scanned with laser power 532 nm with integration

time between 4–50 ms using Bay Spec 3 in 1 Raman Microscope.

The UL-94 vertical flame test was done according to ASTM D3801 with sheet dimensions $130 \times 13 \times 3.2 \text{ mm}^3$. The Limiting Oxygen Index (LOI) was determined according to ASTM D2863-97 with sample size $130 \times 6.5 \times 3 \text{ mm}^3$ using ZR-1 Intelligent Oxygen Index Analyzer.

Cone Calorimeter (Fire Testing Technology Ltd., UK) was carried out according to ISO 5660-1 standard with square specimens ($100 \times 100 \times 3 \text{ mm}^3$). Samples were wrapped in Al foil and irradiated at an external heat flux of 35 kW/m^2 . The fire performance index (FPI) was calculated using Equation (2):

$$FPI = \frac{t_{\text{ign}}}{PHRR} \quad (2)$$

where t_{ign} is the time to ignition and $PHRR$ is the peak heat release rate of PLA, PLA/P-TAB, and PLA/P-TAB/WF biocomposites. Similarly, the fire growth index was also determined according to Equation (3):

$$FGI = \frac{PHRR}{t_p} \quad (3)$$

where $PHRR$ is the peak heat release rate and t_p is time to peak heat release of neat PLA, and PLA/P-TAB, and PLA/P-TAB/WF biocomposites.

The mechanical property was carried out on INSTRON 5566 using $\pm 500 \text{ N}$ load cell according to ASTM D882 – 12 standard at 5 mm/min with five dumb-bell shaped specimens ($50 \times 4 \times 0.84 \text{ mm}^3$) for each composition.

3. Results and discussion

3.1. Structural characterization P-TAB

The FTIR spectra of P-TAB was taken, and the result is shown in Figure 2a. The small narrow absorption peaks around 3480 cm^{-1} are attributed to the stretching vibrations of the secondary amine (N–H), with its bending mode around 1598 cm^{-1} . The peaks belonging to the aromatic ring modes appeared at $1620\text{--}1510 \text{ cm}^{-1}$ [41]. The absorption band around $3050\text{--}2930 \text{ cm}^{-1}$ corresponds to C–H stretching vibrations with their bending mode at 1495 cm^{-1} in P-TAB. The absorption peak of the P=O bond can be seen at 1183 cm^{-1} while the sharp peak at 946 cm^{-1} is ascribed to the stretching vibration of the P–N bond in P-TAB [42, 43] with the prominent C–N peak at 1389 cm^{-1} . The ^1H spectrum of P-TAB is shown in Figure 2b. The doublet around 9.25 and 9.23 ppm together with the multiplet at 8.59–8.52 and 8.82–8.53 ppm belongs to the aromatic ring in ABT, while the singlet shift around 9.15 ppm could be attributed to the resonance vibrations of the hydrogen atom of the secondary amine in P-TAB. The ^{13}C NMR spectrum further confirms the success of the synthetic process by the count of the carbon atoms present in P-TAB (as shown in the experimental section) The ^1H , ^{13}C NMR and the presence of P–N and C–N peaks in FTIR spectra demonstrates that P-TAB was successfully synthesized.

3.2. Thermal properties of P-TAB, WF, and its PLA biocomposites

The thermal properties of P-TAB, WF, and PLA/P-TAB/WF composites are presented in Figure 3.

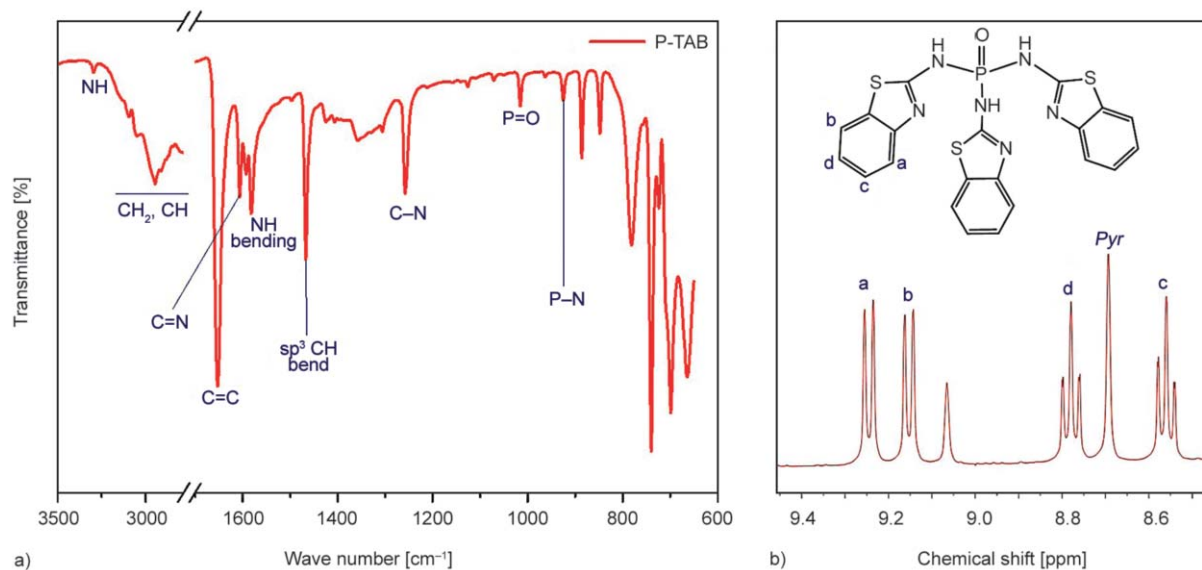


Figure 2. (a) FTIR spectra of P-TAB (b) ^1H NMR of P-TAB.

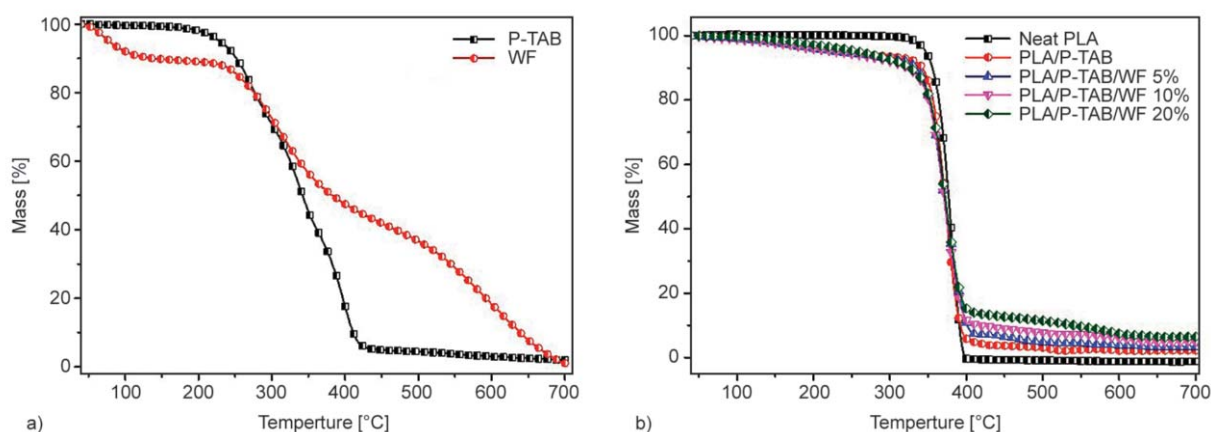


Figure 3. (a) TGA of P-TAB, and WF, (b) TGA of PLA, PLA/P-TAB, PLA/P-TAB/WF composites.

P-TAB presented three T_{-max} decomposition peaks at 276, 339 and 396 °C respectively; while WF exhibited two major T_{-max} peaks at 307, 594 °C (Figure 2, Table 2). Similarly, the onset decomposition temperature ($T_{-5\%}$) for P-TAB and WF at lower temperatures compared to neat PLA. The early mass loss for P-TAB is ascribed to the loss of crystal water and possible decomposition by remnants of unreacted monomers. The first stage mass loss at T_{-max} is due to the decomposition of the secondary amine groups. The second T_{-max} peak is due to the release of PO· radicals, sulfur and nitrogen oxides followed by the oxidation of unstable chars resulting from the carbonization process and subsequent formation of stable char residues. With regards to WF, the early mass loss below 150 °C is ascribed to the evaporation of adsorbed/crystal water and possible physical defects in the amorphous regions of the polymer chains during usage and homogenization [44]. The T_{-max} decomposition peak around 307 °C is attributed to the denaturing and degradation of the keratin molecules, followed by the cleaving of the disulfide bonds around 596 °C and subsequent char formation [26]. The keratin structural protein in WFs contains high

levels of sulfur and nitrogen, which creates char stability under high thermal conditions [45]. The maximum mass loss (M.M.L.) for WF is approximately twice that of P-TAB, which suggests high thermal stability of WF even at T_{-max} . However, the char yield for P-TAB was higher (2.05 wt%) compared to WF (1.06 wt%). The marginally higher char residue of P-TAB is due to the enhanced condensed phase mechanism of phosphorus. P-TAB (constant weight fraction 3%) and WF (different weight fractions of 5, 10, 20%) were mixed with PLA/P-TAB composites, and the thermal properties were studied. The PLA/P-TAB/WF composites presented early degradation with the increasing content of P-TAB and WF (Table 2).

Unlike P-TAB and WF additives alone, the composites (PLA/P-TAB/WF) displayed only one T_{-max} peak at a relatively lower temperature compared with neat PLA (Table 2). The early T_{-5} and T_{-max} peaks are attributed to the early decomposition of the FR in the composites leading to the release of gaseous products which retire the degradation of PLA. The maximum mass change (M.M.C.) at T_{-max} of neat PLA was higher (−2.8%) compared PLA/P-TAB or

Table 2. TGA and DTG data of P-TAB, WF and PLA/P-TAB/WF composites.

Sample	$T_{-5\%}$ [°C]	$T_{-max\%}$ peak 1/2/3 [°C]	T_{-50} [°C]	M.M.C. [%]	C.R. [wt%]
P-TAB	229.5	276/339/396	342.5	−0.7	2.1
WF	202.5	307/594	385.1	−0.3	1.1
PLA	344.8	380.1	376.6	−2.8	0.1
PLA/P-TAB	261.6	373.6	372.4	−2.2	1.0
PLA/P-TAB/WF 5%	214.2	372.2	371.6	−1.6	3.3
PLA/P-TAB/WF 10%	213.6	371.0	372.9	−1.7	5.0
PLA/P-TAB/WF 20%	212.4	370.3	373.9	−1.8	6.7

C.R. – Char Residue; M.M.C. – Maximum mass change at T_{-max}

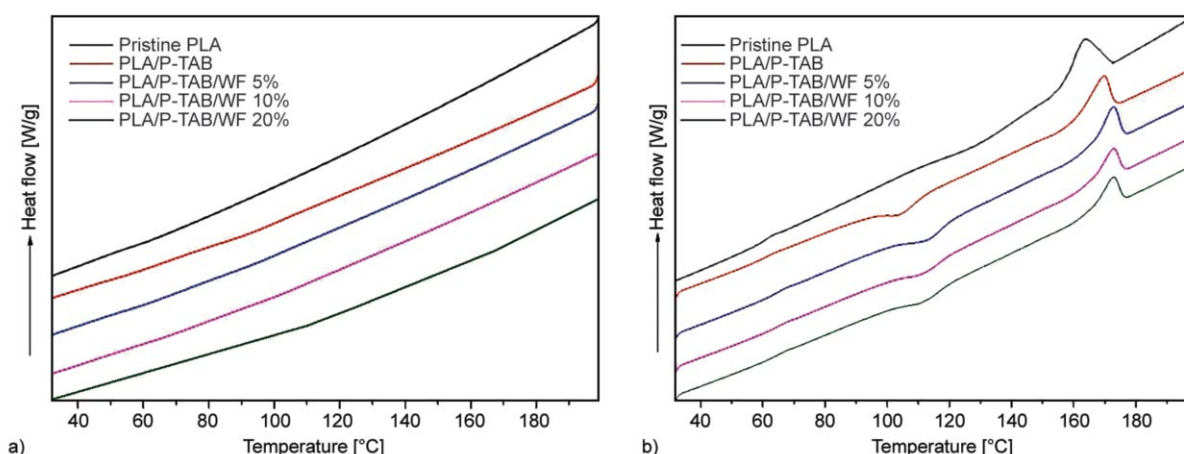


Figure 4. DSC curve of PLA, PLA/P-TAB, and PLA/P-TAB/WF composites: (a) cooling curve from 200 to 35 °C, and (b) second heating from 35 to 200 °C.

PLA/P-TAB/WF composites. With the increase in the content of WF to 5 wt% in the composite, the M.M.C. reduced to -1.6% . However, with further increases in WF content to 10 and 20 wt%, the M.M.C. increased to ca. -1.7 and -1.8% respectively. The char residue (C.R.) of PLA/P-TAB/WF composites increased marginally as the content of WF increases (see Table 2). It is evident from the increases in C.R. content that WF plays a vital role in the formation of char. Compact chars serve as a barrier to heat and reduce gaseous exchanges between the flame zone and the unburnt polymer composites [29]. Generally, the formation of carbonaceous intumescent char often shields and suppresses heat and mass loss rate of the composites and result in reductions in the flame spread and heat reduction [46].

The DSC curves of PLA, PLA/P-TAB, PLA/P-TAB/WF composites are presented in Figure 4 with the related data in Table 3. Typically, no peaks were observed in the non-isothermal cooling process from the molten state as shown in Figure 4a due to the faster cooling rate and the stereochemistry of the PLA used. In the second heating scan, however, obvious exothermic peaks for PLA, PLA/P-TAB, PLA/P-TAB/WF composites were detected. Also, the cold crystallization PLA/P-TAB reduced significantly

compared to pristine PLA as shown in Table 3. However, with the introduction of WF at various quantities, the cold crystallization temperature increased. This phenomenon suggests that the polymer chains gain sufficient mobility to arrange themselves into ordered structure at lower temperature when P-TAB was introduced into PLA, hence the ability to crystallize at lower temperature than pristine PLA, whereas an additional energy (increased temperature) was required for the polymer chains to gain enough mobility to arrange themselves into similar ordered structure when WF was introduced at different loadings. Similarly, a minor increase in the melting temperature of PLA/P-TAB and its WF reinforced composites were observed (see Figure 4b and Table 3). The marginal rise in melting temperature is due to the increased intrinsic defects in the crystal sizes of PLA caused by the presence of P-TAB and WF [37]. The percentage crystallinity (χ_c) for PLA reduced marginally with the introduction of P-TAB into PLA, however, when WF was introduced in various amounts, the χ_c decreased steadily as shown in Table 3. The steady decrease in χ_c is due to the disruption of PLA crystals by P-TAB and WF [36, 38]. With regards to the T_g , no apparent changes were observed in WF reinforced PLA/FR composites and neat PLA

Table 3. Calorimetry data derived from the second heating measured after cooling from the melt.

Sample	T_g [°C]	T_c [°C]	ΔH_c [J/g]	T_m [°C]	ΔH_m [J/g]	χ_c [%]
PLA	62.5	139.5	3.8	166.9	45.8	48.9
PLA/P-TAB	61.6	98.2	22.4	169.9	44.2	47.2
PLA/P-TAB/WF 5 %	61.6	103.7	23.7	172.1	40.7	43.5
PLA/P-TAB/WF 10 %	60.5	105.4	22.7	172.5	33.2	35.5
PLA/P-TAB/WF 20%	60.4	104.7	23.2	172.6	32.1	34.3

(see Table 3), indicating the inconsequential effect of P-TAB or WF on the segmental mobility of PLA.

3.3. Burning behavior

The burning behavior of the samples were investigated by vertical burning tests (VBT), and the results are presented in Table 4. When the samples were torched, the neat PLA dripped heavily (melt flame dripping) and burned the cotton placed beneath. The sample had sustained burning and therefore, resulted in no rating (NR). The PLA/P-TAB delayed the ignition time and had faster self-extinguishing time after the first and second flame applications with significantly fewer polymer drops (no flaming). Therefore, a V-1 rating was attained. Also, the flame was less fierce compared to neat PLA. The effect of WF on the burning resistance and melt dripping phenomenon was eminent in the PLA/P-TAB/WF composites because the dripping, and intensity of the flame reduced immensely but the flame timeout prolonged compared to the PLA/P-TAB composite, especially for the 5 and 10 wt% WF loading. The phenomenon is due to extreme gas evolution of products like NH_3 , CO, and H_2S by WF macromolecular chains during degradation into lighter products and volatile compounds which react with oxygen in the gas phase. Therefore, the samples could only achieve a V-2 rating. During the 10 s flame application, the PLA/P-TAB/WF samples formed fragile residual char, which fell off due to the relatively prolonged burning. However, when the content of WF in PLA/P-TAB composite increased to 20 wt%, a heavy char formed at the tip of the polymer and impeded further combustion. The dripping phenomenon was curtailed, and a comparatively faster self-extinguishing time was attained as shown in Table 4. Therefore, a V-0 rating was obtained. The enhanced charring effect of PLA/P-TAB/WF 20% composites is due to

the combined effect of the sulfur, amino acids, nitrogen, and acidic carboxyl groups in WF and the phosphorus in P-TAB, which act predominantly in the condensed and the gas phases to reduce the exchange of pyrolysis gases and oxygen.

3.4. Forced flame combustion

The combustion behavior of PLA, PLA/P-TAB, and PLA/P-TAB/WF composites were studied with cone calorimeter, and the results are shown in Table 5. The time to ignition (TTI), peak heat release rate (PHRR), total heat release (THR), total smoke release (TSR), CO and CO_2 produced were assessed and the FPI and the FGI were determined. Neat PLA had a TTI of ca. 40 s, a PHRR of ca. 408 kW/m^2 , and THR of ca. 49 MJ/m^2 . When 3 wt% P-TAB was introduced into PLA, the TTI increased from ca. 40 to 50 s. With the addition of WF into PLA/P-TAB composite, the TTI decreased by 22.5%. This trend continued with the increasing WF content in the composite until it reduced similarly to neat PLA. More so, significant reductions in PHRR was observed when 3 wt% P-TAB was added to PLA. Typically, ca. 35.5% reductions in PHRR was observed whereas the THR reduced marginally by ca. 8.2% (Table 5). Subsequently, the HRR increases marginally with the introduction of WF, but the THR decreased continuously with WF loading (Table 5). The increase in PHRR suggests increasing fire intensity whereas the decrease in THR indicates a reduction in heat generated. Although the fire intensity increased, the total heat generated was low due to a shorter burning time. With regards to the mass loss of PLA and its FR composite, the various PLA/P-TAB/WF composites presented early mass loss similar to the phenomenon observed in TGA during combustion in CCT. The early mass loss leads to the release of inert nitrogen oxides, phosphorus radicals and material

Table 4. LOI and representative UL 94 data for PLA, PLA/P-TAB and PLA/P-TAB/WF composites.

Sample	LOI [%]	UL 94 Vertical test			
		Flame timeout [s]		Ign. of cotton/dripping	Rating
		T_1	T_2		
PLA	19.5	12±1	22±2	Yes/Yes (H.D.)	N. R.
PLA/P-TAB	29.8	3±1	2±1	No/Yes (L.D)	V-1
PLA/P-TAB/WF 5%	24.7	9±1	12±1	No/Yes (L.D)	V-2
PLA/P-TAB/WF 10%	26.3	5±1	6±1	No/Yes (L.D)	V-2
PLA/P-TAB/WF 20%	28.5	3±1	2±1	No/No	V-0

Note: H.D.: Heavy dripping, L.D.: Light dripping

Table 5. Cone calorimetry data for P-TAB/PLA and P-TAB/PLA/WF composites at heat flux of 35 kW/m².

Sample	TTI [s]	PHRR [kW/m ²]	THR [MJ/m ²]	PCOP [g/s]	PCO ₂ P [g/s]	AEHC [MJ/kg]	C.R [wt%]
PLA	40±2	408±13	49±3	0.0031±0.001	0.39±0.01	16.7±2.1	1.7±0.5
PLA/P-TAB	50±2	264±6	45±2	0.0012±0.006	0.26±0.02	13.3±0.3	6.7±0.6
PLA/TAB/WF 5%	49±1	277±9	40±2	0.0038±0.003	0.27±0.04	13.6±1.1	11.2±0.4
PLA/P-TAB/WF 10%	48±2	290±12	34±1.2	0.0050±0.002	0.29±0.05	14.8±1.6	16.4±0.1
PLA/P-TAB/WF 20%	40±2	302±19	28±1.5	0.0044±0.004	0.30±0.05	15.1±1.2	21.3±0.2

C.R.: Char residue

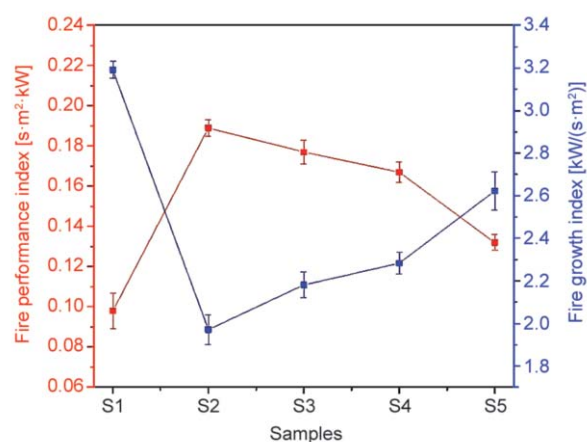
charring by the WF to increase char production. However, the mass loss rate reduced and eventually became stable after the 180 s resulting in a steady increase in char residue with the increasing content of WF. Inopportunately, the char residues appeared frail and therefore was not be able to serve as a complete protective barrier to insulate the underlying polymer from further burning, hence increase in *PHRR* – although the *THR* reduced.

The presence of most FRs in polymers results in increased CO, CO₂, dioxins, HCN production during combustion [47]. The peak CO₂ and CO produced during the combustion process are presented in Table 5. The CO₂ production followed a similar trend to the *PHRR* due to the high conversion of partial oxidization product (CO) to full oxidization product (CO₂) [42]. The CO production for FR PLA occurred mainly in the first 25 to 50 s with the PLA/P-TAB and PLA/P-TAB/WF composites having the lowest PCOP. However, towards the end of the combustion process (around 180–250 s), the CO production for PLA/P-TAB and PLA/P-TAB/WF composites increased marginally compared to the neat PLA due to smoldering resulting from incomplete combustion due to the condensed phase mechanism of P-TAB and conversely, the extreme gas phase mechanism of WF. The increased char residue induced by WF wasn't compact enough to reinforce the condensed phase chemistry of phosphorus, thus resulting in the evolution of a higher CO.

Effective heat of combustion is the measure of the amount of heat released from a burning material per unit of sample burned during combustion in the cone calorimeter test. Low average effective heat of combustion values usually indicates a delay in ignition times and subsequent improvement in fire safety of polymeric materials. PLA/P-TAB had the lowest AEHC as shown in Table 5. When WF was introduced, the AEHC increased marginally. It is imperative to state that PLA/P-TAB alone improved the fire safety of the composites compared to PLA/

P-TAB/WF composites. However, generally, the AEHC of PLA/P-TAB/WF was lower than neat PLA – indicating a general FR efficiency of the phosphorus/WF system in improving the fire safety of PLA.

Figure 5 shows the FPI and the FGI of pristine PLA, PLA/P-TAB, and PLA/P-TAB/WF composites. Higher FPI and lower FGI values relate to enhanced fire safety for polymeric materials. Typically, the introduction of 3 wt% P-TAB into PLA led to a significant increase in FPI. When 5 wt% WF was introduced, the FPI decreased from 0.189 to 0.177 s·m²/kW. As the content of WF increased further to 10 and 20 wt% in the composites, the FPI decreases steadily to 0.167 and 0.132 s·m²/kW. Despite the obvious decreases resulting from the increasing WF content in PLA/P-TAB, the 20 wt% WF loading is 34.7% higher than that of neat PLA – indicating increased fire safety by the PLA/P-TAB/WF composites. In the same way, the FGI value for PLA/P-TAB composite decreased by 38.2%, however, with the introduction of 5 wt% WF, the FGI declined to 31.7%, signifying increased fire risk compared to PLA/P-TAB composite. When the content of WF in PLA/P-TAB composite increased to 10, and 20 wt%, the FGI values

**Figure 5.** FGI/FPI of PLA, PLA/P-TAB and PLA/P-TAB/WF composites (SI: Pristine PLA, S2: PLA/P-TAB, S3-5: various WF loading in PLA/P-TAB composites).

decreased further to 28.5 and 17.8% respectively. This phenomenon is consistent with the trend observed in PHRR. The presence of WF in PLA/P-TAB composites catalyzes early combustion and intensifies fire growth but leads to faster self-extinguishment, and at the same time reduces heat generation and stops melt dripping. It is important to state that despite the worsening FGI value because of WF addition, the composites polymers showed improved flame retardancy compared to neat PLA.

3.5. Residual char analysis

The microstructure of the char residues after the cone calorimeter test (CCT) were studied to understand the effects of WF and P-TAB on the composite's char formation, and its correlation with the FR trend observed in CCT, LOI, and UL 94 tests. The SEM micrographs shown in Figure 6. Neat PLA had less residue (predominantly made up of soot) while

PLA/P-TAB composite had a significant amount of char residue after combustion. The influence of WF on intumescent char formation was observed with the increasing WF content. The charring effect of PLA/P-TAB/WF composites is due to the sulfur and amino acids in WF and P-TAB, in addition to the formation of phosphoric acids and the sulfonic groups during the endothermal decomposition process [29]. From the SEM image of PLA/P-TAB shown in Figure 6a, a condensed char structure that can effectively reduce the diffusion of organic volatiles and heat can be observed, although it contains some nano-size pores/bubbles. Conversely, a more porous, less compact char structure with micron-sized fissures can be observed in the PLA/P-TAB/WF composites. The many fissures are obviously detrimental to fire growth and gaseous/smoke control because they could effectively serve as a diffusion channel for oxygen entry into the flame zone, and the release of pyrolysis

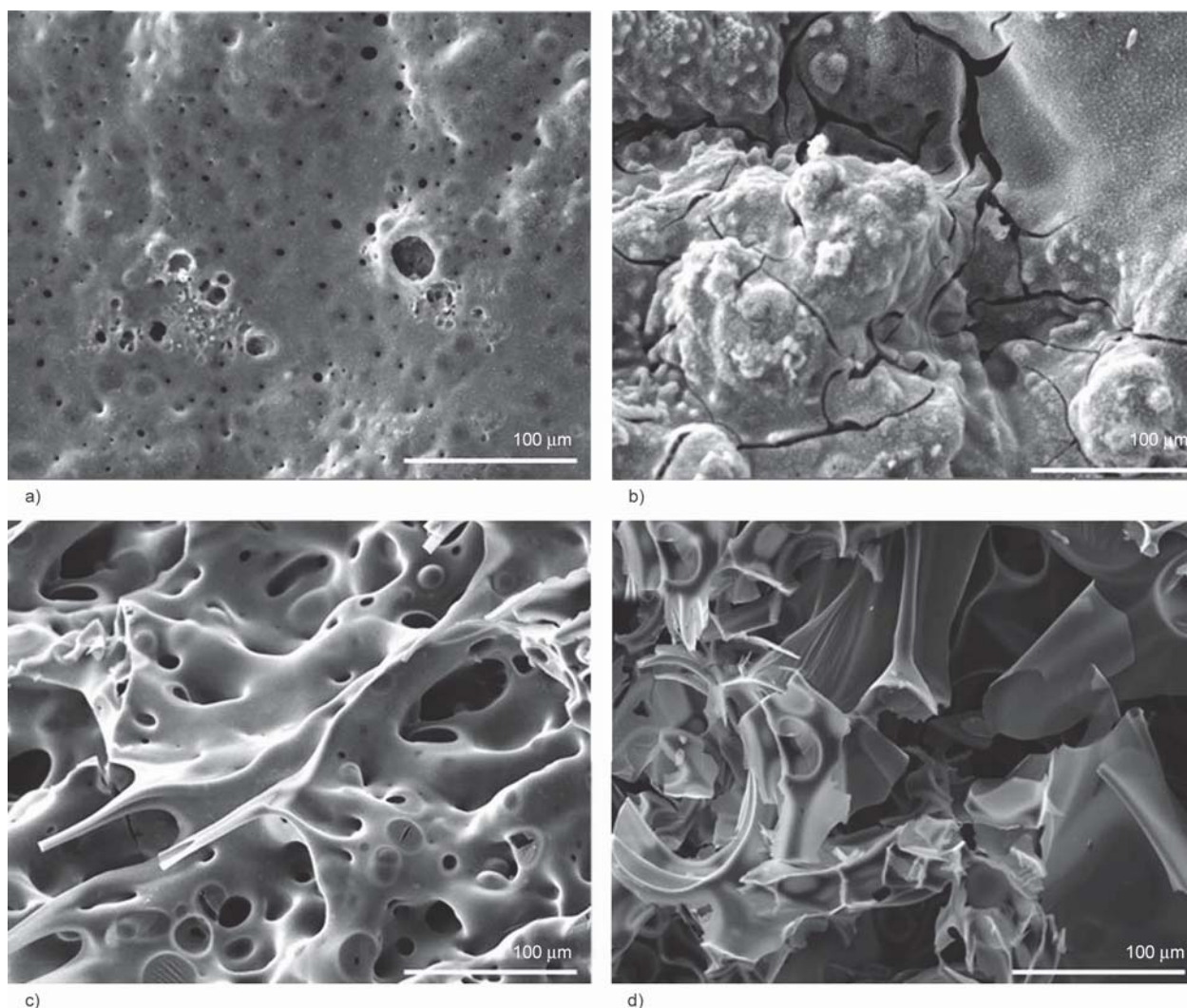


Figure 6. SEM images of: (a) PLA/P-TAB, (b) PLA/P-TAB/WF 5%, (c) PLA/P-TAB/WF 10% and (d) PLA/P-TAB/WF 20% composites.

products as well as aid heat exchanges between the flame zone and the underlying polymer. This phenomenon could result in increased heat release and fire growth. The porous char structure is attributed to the fragile mechanical resistance of the WF chars. This phenomenon is consistent with the increased HRR, COP CO₂P, FPI and FGI values observed in the cone calorimeter test with the increasing WF content.

The FTIR spectra of the residual chars were taken after CCT, and the results are shown in Figure 7. Peaks corresponding to CH vibrations can be found around 2921–2847 cm⁻¹. The peaks around 1575–1440 cm⁻¹ relate to vibrations of heteroatomic species of decomposed aromatic rings in P-TAB. The distinct peaks around 1452–1428 cm⁻¹ are attributed to C–O and C=O vibrations resulting from the decomposition products of PLA, P-TAB, and WF, while the peak at 1172 cm⁻¹ relates to vibrations of tertiary amide resulting from the decomposition of the proteins from WF. The absorption bands at 1132 and 903 cm⁻¹ are attributed to the stretching vibrations of P=O and P–N groups respectively, while the peak at 1018 cm⁻¹ indicates the existence of S=O groups in the char residue.

Raman spectra of PLA/P-TAB and PLA/P-TAB/WF residual chars are shown in Figure 7. The G band (1600 cm⁻¹) relates to the in-plane vibrations of graphite carbons while the D band at 1338 cm⁻¹ indicates to the presence of amorphous carbons [48]. The area of D divided by G (I_D/I_G) relates to the extent of graphite or amorphous content present in the residual chars [49]. Mostly, higher I_D/I_G values indicate

the presence of more amorphous chars, while the reverse is an indication of more graphite chars [50]. PLA/P-TAB had the lowest I_D/I_G value with the P-TAB/WF 20% having the highest I_D/I_G value (see Figure 7b). The phenomenon suggests an increase in amorphous char content after the introduction of WF. The increasing amorphous contents decrease the thermal stability/rigidity of the residue char which can allow for the exchange of organic volatiles and oxygen in the flame zone. Such occurrence resulted in increased fire growth rate and the high PHRR observed from CCT. The presence of heteroaromatic elements in the residual char is confirmed by the shoulder peaks around 755 and 1155 cm⁻¹ which are attributed to C–N and remnants of heteroaromatic species in the aromatic ring of P-TAB.

Based on the macro/microstructure, FTIR and the Raman spectra, the FR mechanism can be attributed to the condensed phase FR actions of phosphorus-nitrogen-sulfur moieties in P-TAB and the predominantly gas phase inhibition of WF [51–53]. During combustion, the N–S moieties degenerate into nitrogen and sulfur oxides that dilute the combustible gases [54]. In addition, the phosphorus moiety generates phosphorus radicals that suppress the evolution of volatile radicals while at the same time acting in the condensed phase to promote char formation. Also, the sulfur component in both P-TAB and WF contribute to the FR action by forming sulfonic acids in the flame when water is produced, in addition to the hydrolytic scissions of keratin polypeptides in WF. During endothermic decomposition of WF, the macromolecular chains decomposed into lighter

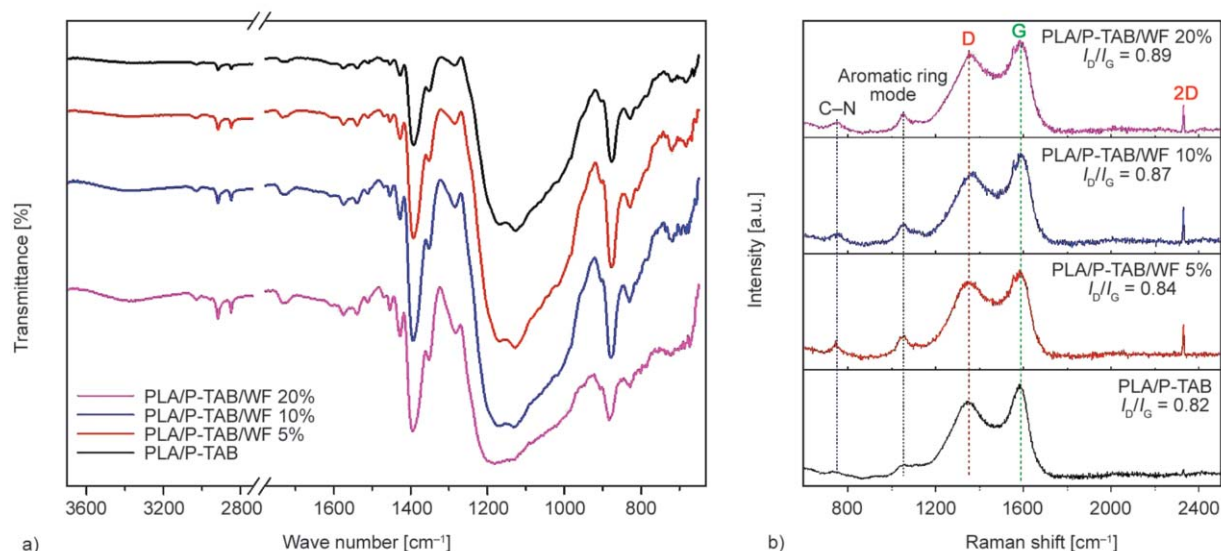


Figure 7. (a) FTIR spectra, and (b) Raman spectra of char residues after CCT.

products and volatile compounds like NH_3 , CO , and H_2S that react with oxygen in the gas phase, resulting in various oxidation products [55]. These processes lead to the formation of crosslinked char layers in the condensed phase, however, not compact enough due to the excessive evolution of pyrolysis gases products from WF. As a result, the char generated is not compact enough to serve as a complete barrier to the suppression of other volatile pyrolysis products [51] during combustion; hence the increases in PHRR, CO , and CO_2 .

3.6. Pyrolysis gaseous product analysis

The pyrolysis gaseous products of PLA, PLA/P-TAB, and PLA/P-TAB/WF biocomposites during the thermal degradation process were investigated by TG-FTIR, and the results are presented in Figure 8. The FTIR spectrum of PLA/P-TAB and PLA/P-TAB/WF PLA biocomposites did not show any noticeable difference from that of neat PLA, implying that similar volatile gases were released during the thermal degradation process. The gaseous absorption products unique to P-TAB or WF were not noticeable, possibly due to the overlapping of the absorptions bands from the pyrolysis products of PLA. From Figure 8a,

the gaseous pyrolysis products unique to PLA occurred around 3506 , 2900 – 3000 , 2350 , and 2114 – 2182 cm^{-1} , which are attributed to the evolution of water, hydrocarbons, CO_2 and CO respectively [56]. The absorbance around 1759 and 1100 – 1250 cm^{-1} are ascribed to carbonyl compounds and aliphatic ester groups respectively. Similar peaks were recorded for the PLA/P-TAB and PLA/P-TAB/WF 20% composites but at reduced absorption intensities as shown in Table 6. An overall reduction of evolved gaseous products during pyrolysis were obtained by the composites compared to neat PLA. A slight increase in total evolved gaseous product for PLA/P-TAB/WF 20% was observed similar to the phenomenon observed from CCT gaseous products characterization. A similar occurrence was observed in total hydrocarbons, carbonyl compounds, and CO with the introduction of WF as shown in Table 6. Generally, PLA/P-TAB gave the lowest pyrolysis gaseous products compared to neat PLA and PLA/P-TAB/WF composites. When WF was introduced, a marginal increase in total hydrocarbons, carbonyl compounds, and CO was observed. This phenomenon is due to the increased gas phase mechanism of WF due to the abundant pyrolysis volatile products

Table 6. Absorbance intensities of pyrolysis products of PLA and composites at maximum decomposition temperature.

Pyrolysis gases	Neat PLA [a.u.]	PLA/P-TAB [a.u.]	PLA/P-TAB/WF 20% [a.u.]
Carbonyl compounds	9.22	5.51	7.75
Hydrocarbons	0.203	0.130	0.558
Carbon monoxide	Peak 1 = 0.071 Peak 2 = 0.012	Peak 1 = 0.052 Peak 2 = 0.016	Peak 1 = 0.067 Peak 2 = 0.023
Total absorption	1.28	0.81	1.02

Note: Peak one and two occurred at approximately 19 minutes 36 seconds, and 48 minutes 46 seconds respectively during pyrolysis.

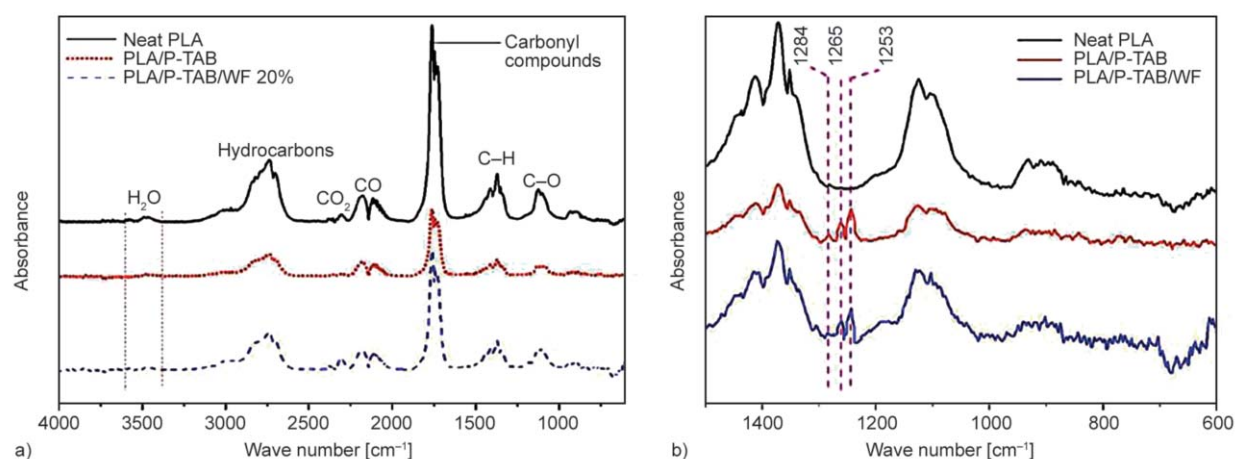


Figure 8. TG-IR absorbance spectra of pyrolysis products of: a) Neat PLA, PLA/P-TAB, PLA/P-TAB/WF 20%, (b) phosphorus radicals evolved.

of NH_3 , CO , and H_2S macromolecular chains of WF during thermal decomposition and the porous nature of its residual chars as observed from the SEM micrograph in Figure 6c, 6d). Also, the absorption bands around 1284 , 1265 and 1253 cm^{-1} in PLA/PTAB and PLA/P-TAB/WF 20 wt% composites are due to evolved pyrolysis gaseous products of phosphorus radicals such as $\text{P}=\text{O}\cdot$, $\text{P}-\text{O}\cdot$, and $\text{P}-\text{OH}\cdot$ fragments respectively; which are clearly missing from neat PLA [56] at the maximum decomposition temperature (Figure 8b).

3.7. Mechanical properties

FRs generally reduce the flammability of polymeric materials but at the same time can have a detrimental effect on the mechanical properties of composites, which might affect their engineering end use [4, 57]. As a result, the tensile properties of WF reinforced PLA/P-TAB composites were investigated, and the results are shown in Figure 9. The tensile strength,

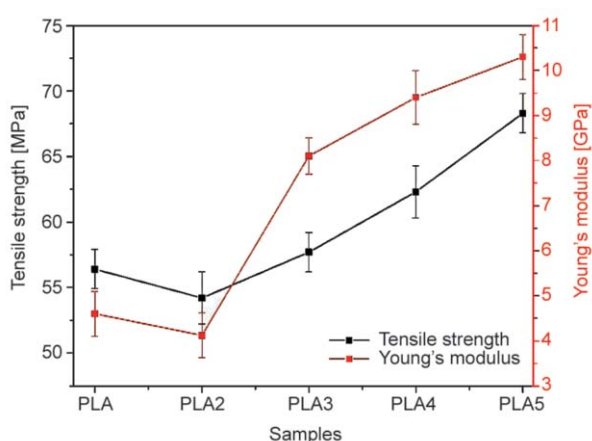


Figure 9. Tensile strength vs. Young's modulus of PLA, PLA/P-TAB, PLA/P-TAB/WF composites. (Note: PLA: neat PLA; PLA 2: PLA/P-TAB; PLA 3: PLA/P-TAB/WF 5%; PLA 4: PLA/P-TAB/WF 10%; PLA 5: PLA/P-TAB/WF 20%.

elongation at break and the Young's modulus reduced marginally by ca. 3.9, 8.1, and 4.5% respectively, with the addition of 3 wt% of P-TAB into PLA. When certain percentages of WF (5, 10, and 20 wt%) introduced into PLA/P-TAB composites, the tensile strength increased by ca. 3.5, 10.4, 26.6% respectively. Similarly, the Young's modulus also increased considerably as shown in Figure 9. Nevertheless, the elongation at break of the PLA/P-TAB, and its WF composites reduced. The apparent reduction in elongation at break is due to the increased rigidity in the organic-inorganic interface between PLA, P-TAB, and WF. The increase in tensile strength by PLA/P-TAB/WF composites can be attributed to the reinforcement effect of short WF in the composites.

To understand the reinforcement effect of WF in PLA/P-TAB composites, SEM micrographs of the specimen fracture surface (cross-section) after the tensile test was taken. Neat PLA, PLA/P-TAB, and PLA/TP-TAB/WF 20% composites were studied, and the results are shown in Figure 10. Compared to neat PLA, PLA/P-TAB had micron size pores and interfacial defects. The interfacial defects and the micron size pores ultimately contributed to the reduced tensile strength, elongation at break, and Young's modulus observed in PLA/P-TAB composites. The pores created porous amorphous fractions within the PLA matrix which thus weakened the molecular cohesion of PLA chains in the matrix. For the WF reinforced PLA/P-TAB composites, the PLA matrix around WF appeared captured and dissipated earlier, thus transferring the load to WF in the matrix. Therefore, obvious fiber pulls/breaks could be observed, indicating the reinforcement effect of WF for PLA/P-TAB composites. However, the tensile strength and the elongation at break also depends mainly on the alignment of WF along the axis of the pull

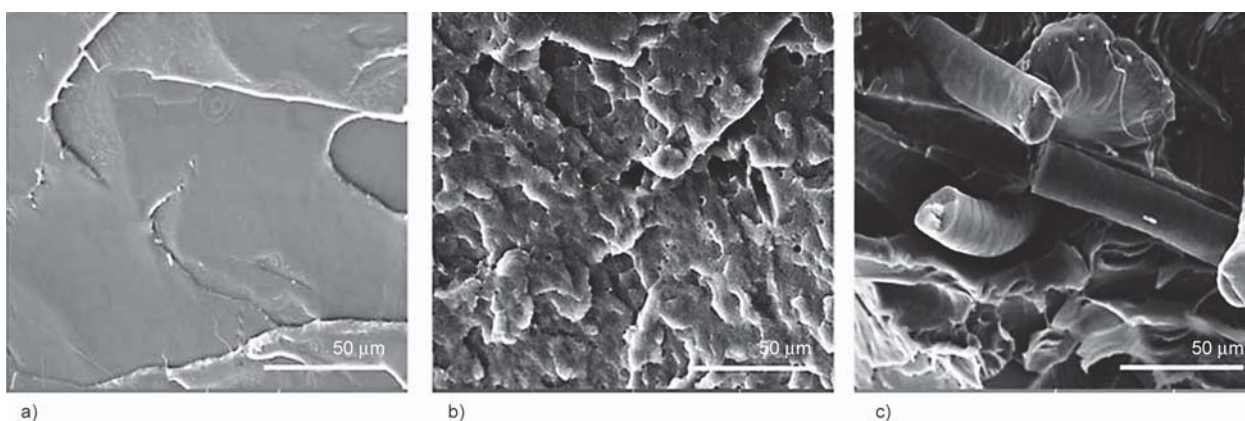


Figure 10. SEM images of fracture surface from the tensile test: (a) neat PLA, (b) PLA/P-TAB, (c) PLA/P-TAB/WF 20%.

because the composite could break easily at its weakest point, which is the interfacial region between WF and the PLA/P-TAB matrix across the pulling direction. Depending on the priority of the specific mechanical properties desired (whether high mechanical strength to the detriment of elongation or vice versa), the PLA/TP-TAB/WF composites could be tailored to perform without compromising the FR properties. For instance, the elongation at break could be improved by the incorporation of a plasticizer while maintaining the excellent fire retardancy and high tensile strength.

4. Conclusions

The synthesis and application of phosphorus-nitrogen-sulfur containing FR (phenylphosphonic 3(2-aminobenzothiazole) (P-TAB) and its combination with recycled short wool fibers for simultaneous FR and tensile strength enhancement of PLA biocomposites were reported. The composites were prepared by solvent mixing and compression molding and characterized extensively. FTIR, ^1H and ^{13}C NMR confirm the successful synthesis of phenylphosphonic 3(2-aminobenzothiazole) (P-TAB). The combination of P-TAB with recycled wool fiber (WF) into PLA resulted in significant improvement in flame retardancy and tensile strength of the polymer composites (PC). Typically, the PHRR improved by ca. 35.5%, the THR by ca. 8.2%, and AEHC by ca. 24% with 3 wt% P-TAB loading. When WF was introduced, a marginal decline in PHRR and AEHC were observed. SEM and Raman spectroscopic study of the char residue revealed the development of more loosely bound amorphous char with micron size fissures with the increasing content of WF, which served as an escape route for heat and pyrolysis gases hence the increases in PHRR and AEHC. However, the WF reinforced PLA/P-TAB composite had improved FR performance compared to neat PLA due to apparent increases in THR, PHRR, FPI, and FGI compared to neat PLA. Also, a higher LOI value of 28.5% and a V-0 rating was obtained when 20% WF was introduced into PLA/P-TAB composites. DSC results showed a gradual reduction in the degree of crystallization with the increasing WF content. TG-FTIR study of evolved gaseous products indicates a significant reduction in total hydrocarbons, carbonyl compounds, and CO produced during thermal degradation.

More importantly, significant improvement in tensile strength and Young's Modulus was observed with the increasing WF content in PLA/P-TAB composites reaffirming the reinforcement effect of WF in preparing advanced functional composites for engineering applications.

Acknowledgements

The authors are thankful for the funding support of GRF project 15208015

References

- [1] Ku H., Wang H., Pattarachaiyakoo N., Trada M.: A review on the tensile properties of natural fiber reinforced polymer composites. *Composites Part B: Engineering*, **42**, 856–873 (2011).
<https://doi.org/10.1016/j.compositesb.2011.01.010>
- [2] Dai Z., Yang Z., Chen Z., Zhao Z., Lou Y., Zhang Y., Liu T., Fu F., Fu Y., Liu X.: Fully biobased composites of an itaconic acid derived unsaturated polyester reinforced with cotton fabrics. *ACS Sustainable Chemistry and Engineering*, **6**, 15056–15063 (2018).
<https://doi.org/10.1021/acssuschemeng.8b03539>
- [3] Yu T., Jiang N., Li Y.: Functionalized multi-walled carbon nanotube for improving the flame retardancy of ramie/poly(lactic acid) composite. *Composites Science and Technology*, **104**, 26–33 (2014).
<https://doi.org/10.1016/j.compscitech.2014.08.021>
- [4] Chen H., Wang J., Ni A., Ding A., Sun Z., Han X.: Effect of novel intumescent flame retardant on mechanical and flame retardant properties of continuous glass fibre reinforced polypropylene composites. *Composite Structures*, **203**, 894–902 (2018).
<https://doi.org/10.1016/j.compstruct.2018.07.071>
- [5] Yallev T. B., Kumar P., Singh I.: Mechanical behavior of nettle/wool fabric reinforced polyethylene composites. *Journal of Natural Fibers*, **13**, 610–618 (2016).
<https://doi.org/10.1080/15440478.2015.1093576>
- [6] Zini E., Scandola M.: Green composites: An overview. *Polymer composites*, **32**, 1905–1915 (2011).
<https://doi.org/10.1002/pc.21224>
- [7] Zhao D., Zhou Z.: Applications of lightweight composites in automotive industries. in 'Lightweight materials from biopolymers and biofibers' (eds.: Yang Y., Xu H., Yu X.) American Chemical Society, Vol 1175, 143–158 (2014).
<https://doi.org/10.1021/bk-2014-1175.ch009>
- [8] Mochane M. J., Mokhena T. C., Mokhothu T. H., Mtibe A., Sadiku E. R., Ray S. S., Ibrahim I. D., Daramola O. O.: Recent progress on natural fiber hybrid composites for advanced applications: A review. *Express Polymer Letters*, **13**, 159–198 (2019).
<https://doi.org/10.3144/expresspolymlett.2019.15>

- [9] Al-Oqla F. M., Sapuan S. M.: Natural fiber reinforced polymer composites in industrial applications: Feasibility of date palm fibers for sustainable automotive industry. *Journal of Cleaner Production*, **66**, 347–354 (2014).
<https://doi.org/10.1016/j.jclepro.2013.10.050>
- [10] Thakur V. K., Thakur M. K., Gupta R. K.: Review: Raw natural fiber-based polymer composites. *International Journal of Polymer Analysis and Characterization*, **19**, 256–271 (2014).
<https://doi.org/10.1080/1023666X.2014.880016>
- [11] Negawo T. A., Polat Y., Buyuknalcaçi F. N., Kilic A., Saba N., Jawaïd M.: Mechanical, morphological, structural and dynamic mechanical properties of alkali treated Ensete stem fibers reinforced unsaturated polyester composites. *Composite Structures*, **207**, 589–597 (2019).
<https://doi.org/10.1016/j.compstruct.2018.09.043>
- [12] Friedrich K., Almajid A. A.: Manufacturing aspects of advanced polymer composites for automotive applications. *Applied Composite Materials*, **20**, 107–128 (2013).
<https://doi.org/10.1007/s10443-012-9258-7>
- [13] Koronis G., Silva A., Fontul M.: Green composites: A review of adequate materials for automotive applications. *Composites Part B: Engineering*, **44**, 120–127 (2013).
<https://doi.org/10.1016/j.compositesb.2012.07.004>
- [14] Irving P. E., Soutis C.: *Polymer composites in the aerospace industry*. Woodhead, Sawston (2014).
<https://doi.org/10.1016/C2013-0-16303-9>
- [15] Siengchin S.: Potential use of ‘green’ composites in automotive applications. *Express Polymer Letters*, **11**, 600 (2017).
<https://doi.org/10.3144/expresspolymlett.2017.57>
- [16] Kim N. K., Dutta S., Bhattacharyya D.: A review of flammability of natural fibre reinforced polymeric composites. *Composites Science and Technology*, **162**, 64–78 (2018).
<https://doi.org/10.1016/j.compscitech.2018.04.016>
- [17] Yurddaskal M., Celik E.: Effect of halogen-free nanoparticles on the mechanical, structural, thermal and flame retardant properties of polymer matrix composite. *Composite Structures*, **183**, 381–388 (2018).
<https://doi.org/10.1016/j.compstruct.2017.03.093>
- [18] Couture A., Lebrun G., Laperrière L.: Mechanical properties of polylactic acid (PLA) composites reinforced with unidirectional flax and flax-paper layers. *Composite Structures*, **154**, 286–295 (2016).
<https://doi.org/10.1016/j.compstruct.2016.07.069>
- [19] Chow W., Teoh E., Karger-Kocsis J.: Flame retarded poly(lactic acid): A review. *Express Polymer Letters*, **12**, 396–417 (2018).
<https://doi.org/10.3144/expresspolymlett.2018.34>
- [20] Tawiah B., Yu B., Fei B.: Advances in flame retardant poly(lactic acid). *Polymers*, **10**, 876/1–876/22 (2018).
<https://doi.org/10.3390/polym10080876>
- [21] Yang W., Tawiah B., Yu C., Qian Y-F., Wang L-L., Yuen A. C-Y., Zhu S-E., Hu E-Z., Chen T. B-Y., Yu B., Lu H-D., Yeoh G. H., Wang X., Song L., Hu Y.: Manufacturing, mechanical and flame retardant properties of poly(lactic acid) biocomposites based on calcium magnesium phytate and carbon nanotubes. *Composites Part A: Applied Science and Manufacturing*, **110**, 227–236 (2018).
<https://doi.org/10.1016/j.compositesa.2018.04.027>
- [22] Patrucco A., Cristofaro F., Simionati M., Zoccola M., Bruni G., Fassina L., Visai L., Magenes G., Mossotti R., Montarsolo A., Tonin C.: Wool fibril sponges with perspective biomedical applications. *Materials Science and Engineering: C*, **61**, 42–50 (2016).
<https://doi.org/10.1016/j.msec.2015.11.073>
- [23] Chang H., Li Q., Xu C., Li R., Wang H., Bu Z., Lin T.: Wool powder: An efficient additive to improve mechanical and thermal properties of poly(propylene carbonate). *Composites Science and Technology*, **153**, 119–127 (2017).
<https://doi.org/10.1016/j.compscitech.2017.10.012>
- [24] Forouharshad M., Montazer M., Moghaddam M., Saligheh O., Roudbari B.: Optimization of zirconium acetate on the flame retardant properties of wool. *Journal of Applied Polymer Science*, **125**, 1261–1266 (2012).
<https://doi.org/10.1002/app.35353>
- [25] Basak S., Samanta K. K., Chattopadhyay S. K., Pandit P., Maiti S.: Green fire retardant finishing and combined dyeing of proteinous wool fabric. *Coloration Technology*, **132**, 135–143 (2016).
<https://doi.org/10.1111/cote.12200>
- [26] Conzatti L., Giunco F., Stagnaro P., Patrucco A., Marano C., Rink M., Marsano E.: Composites based on polypropylene and short wool fibres. *Composites Part A: Applied Science and Manufacturing*, **47**, 165–171 (2013).
<https://doi.org/10.1016/j.compositesa.2013.01.002>
- [27] Salatino P., Di Benedetto A., Chirone R., Salzano E., Sanchirico R.: Analysis of an explosion in a wool-processing plant. *Industrial and Engineering Chemistry Research*, **51**, 7713–7718 (2012).
<https://doi.org/10.1021/ie2023614>
- [28] Kim N. K., Lin R. J. T., Bhattacharyya D.: Effects of wool fibres, ammonium polyphosphate and polymer viscosity on the flammability and mechanical performance of PP/wool composites. *Polymer Degradation and Stability*, **119**, 167–177 (2015).
<https://doi.org/10.1016/j.polymdegradstab.2015.05.015>
- [29] Gurunathan T., Mohanty S., Nayak S. K.: A review of the recent developments in biocomposites based on natural fibres and their application perspectives. *Composites Part A: Applied Science and Manufacturing*, **77**, 1–25 (2015).
<https://doi.org/10.1016/j.compositesa.2015.06.007>
- [30] Kilinc F. S.: *Handbook of fire resistant textiles*. Elsevier, Amsterdam (2013).

- [31] Hoang D., Kim J., Jang B. N.: Synthesis and performance of cyclic phosphorus-containing flame retardants. *Polymer Degradation and Stability*, **93**, 2042–2047 (2008).
<https://doi.org/10.1016/j.polymdegradstab.2008.02.017>
- [32] Levchik S. V., Weil E. D.: A review of recent progress in phosphorus-based flame retardants. *Journal of Fire Sciences*, **24**, 345–364 (2006).
<https://doi.org/10.1177/0734904106068426>
- [33] Weil E. D., Levchik S. V., Ravey M., Zhu W.: A survey of recent progress in phosphorus-based flame retardants and some mode of action studies. *Phosphorus, Sulfur, and Silicon and the Related Elements*, **144**, 17–20 (1999).
<https://doi.org/10.1080/10426509908546171>
- [34] Perret B., Schartel B., Stöß K., Ciesielski M., Diederichs J., Döring M., Krämer J., Altstädt V.: Novel DOPO-based flame retardants in high-performance carbon fibre epoxy composites for aviation. *European Polymer Journal*, **47**, 1081–1089 (2011).
<https://doi.org/10.1016/j.eurpolymj.2011.02.008>
- [35] Chen Y., Peng H., Li J., Xia Z., Tan H.: A novel flame retardant containing phosphorus, nitrogen, and sulfur. *Journal of Thermal Analysis and Calorimetry*, **115**, 1639–1649 (2014).
<https://doi.org/10.1007/s10973-013-3461-0>
- [36] Zhao W., Li B., Xu M., Zhang L., Liu F., Guan L.: Synthesis of a novel flame retardant containing phosphorus and sulfur and its application in polycarbonate. *Polymer Engineering and Science*, **52**, 2327–2335 (2012).
<https://doi.org/10.1002/pen.23192>
- [37] Shamsuddin I. M., Jafar J. A., Shawai A. S. A., Yusuf S., Lateefah M., Aminu I.: Bioplastics as better alternative to petroplastics and their role in national sustainability: A review. *Advances in Bioscience and Bioengineering*, **5**, 63–70 (2017).
<https://doi.org/10.11648/j.abb.20170504.13>
- [38] Jiang P., Gu X., Zhang S., Wu S., Zhao Q., Hu Z.: Synthesis, characterization, and utilization of a novel phosphorus/nitrogen-containing flame retardant. *Industrial & Engineering Chemistry Research*, **54**, 2974–2982 (2015).
<https://doi.org/10.1021/ie505021d>
- [39] Tawiah B., Yu B., Cheung W. Y., Chan S. Y., Yang W., Fei B.: Synthesis and application of synergistic azo-boron-BPA/polydopamine as efficient flame retardant for poly(lactic acid). *Polymer Degradation and Stability*, **152**, 64–74 (2018).
<https://doi.org/10.1016/j.polymdegradstab.2018.03.018>
- [40] Valapa R. B., Pugazhenth G., Katiyar V.: Effect of graphene content on the properties of poly(lactic acid) nanocomposites. *RSC Advances*, **5**, 28410–28423 (2015).
<https://doi.org/10.1039/C4RA15669B>
- [41] Morrill L. A., Kammeyer J. K., Garg N. K.: Spectroscopy 101: A practical introduction to spectroscopy and analysis for undergraduate organic chemistry laboratories. *Journal of Chemical Education*, **94**, 1584–1586 (2017).
<https://doi.org/10.1021/acs.jchemed.7b00263>
- [42] Liu W., Chen D-Q., Wang Y-Z., Wang D-Y., Qu M-H.: Char-forming mechanism of a novel polymeric flame retardant with char agent. *Polymer Degradation and Stability*, **92**, 1046–1052 (2007).
<https://doi.org/10.1016/j.polymdegradstab.2007.02.009>
- [43] Shi X., Liao F., Ju Y., Dai X., Cao Y., Li J., Wang X.: Improving the flame retardance and melt dripping of poly(lactic acid) with a novel polymeric flame retardant of high thermal stability. *Fire and Materials*, **41**, 362–374 (2017).
<https://doi.org/10.1002/fam.2389>
- [44] Conzatti L., Giunco F., Stagnaro P., Capobianco M., Castellano M., Marsano E.: Polyester-based biocomposites containing wool fibres. *Composites Part A: Applied Science and Manufacturing*, **43**, 1113–1119 (2012).
<https://doi.org/10.1016/j.compositesa.2012.02.019>
- [45] Liu X., Gu S., Xu W.: Thermal and structural characterization of superfine down powder. *Journal of Thermal Analysis and Calorimetry*, **111**, 259–266 (2013).
<https://doi.org/10.1007/s10973-012-2202-0>
- [46] Yang W., Yang W-J., Tawiah B., Zhang Y., Wang L-L., Zhu S-E., Chen T. B. Y., Yuen A. C. Y., Yu B., Liu Y-F., Si J-Y., Hu E-Z., Lu H-D., Hu K-H., Chan Q. N., Yeoh G. H.: Synthesis of anhydrous manganese hypophosphite microtubes for simultaneous flame retardant and mechanical enhancement on poly(lactic acid). *Composites Science and Technology*, **164**, 44–50 (2018).
<https://doi.org/10.1016/j.compscitech.2018.05.023>
- [47] Stec A. A., Hull T. R.: Assessment of the fire toxicity of building insulation materials. *Energy and Buildings*, **43**, 498–506 (2011).
<https://doi.org/10.1016/j.enbuild.2010.10.015>
- [48] Shi Y., Yu B., Duan L., Gui Z., Wang B., Hu Y., Yuen R. K. K.: Graphitic carbon nitride/phosphorus-rich aluminum phosphinates hybrids as smoke suppressants and flame retardants for polystyrene. *Journal of Hazardous Materials*, **332**, 87–96 (2017).
<https://doi.org/10.1016/j.jhazmat.2017.03.006>
- [49] Ferrari A. C., Robertson J.: Interpretation of Raman spectra of disordered and amorphous carbon. *Physical Review B*, **61**, 14095–14107 (2000).
<https://doi.org/10.1103/PhysRevB.61.14095>
- [50] Wang G., Zhang J., Chang W., Li R., Li Y., Wang C.: Structural features and gasification reactivity of biomass chars pyrolyzed in different atmospheres at high temperature. *Energy*, **147**, 25–35 (2018).
<https://doi.org/10.1016/j.energy.2018.01.025>
- [51] Green J.: Mechanisms for flame retardancy and smoke suppression – A review. *Journal of Fire Sciences*, **14**, 426–442 (1996).
<https://doi.org/10.1177/073490419601400602>

- [52] Qian X., Song L., Hu Y., Yuen R. K. K., Chen L., Guo Y., Hong N., Jiang S.: Combustion and thermal degradation mechanism of a novel intumescent flame retardant for epoxy acrylate containing phosphorus and nitrogen. *Industrial and Engineering Chemistry Research*, **50**, 1881–1892 (2011).
<https://doi.org/10.1021/ie102196k>
- [53] Granzow A.: Flame retardation by phosphorus compounds. *Accounts of Chemical Research*, **11**, 177–183 (1978).
<https://doi.org/10.1021/ar50125a001>
- [54] Hu X-P., Li W-Y., Wang Y-Z.: Synthesis and characterization of a novel nitrogen containing flame retardant. *Journal of Applied Polymer Science*, **94**, 1556–1561 (2004).
<https://doi.org/10.1002/app.20792>
- [55] Popescu C., Segal E., Idoiou C.: A kinetic model for the thermal decomposition of wool. *Thermochimica Acta*, **256**, 419–427 (1995).
[https://doi.org/10.1016/0040-6031\(94\)02186-R](https://doi.org/10.1016/0040-6031(94)02186-R)
- [56] Zhao P., Liu Z., Wang X., Pan Y-T., Kuehnert I., Gehde M., Wang D-Y., Leuteritz A.: Renewable vanillin based flame retardant for poly(lactic acid): A way to enhance flame retardancy and toughness simultaneously. *RSC Advances*, **8**, 42189–42199 (2018).
<https://doi.org/10.1039/C8RA08531E>
- [57] Michler G. H., Balta-Calleja F. J.: *Mechanical properties of polymers based on nanostructure and morphology*. CRC Press, Boca Raton (2016).
<https://doi.org/10.1201/9781420027136>